American Journal of Biological Anthropology

WILEY

AMERICAN JOURNAL OF BIOLOGICAL ANTHROPOLOGY

TECHNICAL NOTE OPEN ACCESS

A Standardized, Three-Dimensional Cropping Protocol for Analyzing the Medial Epicondyle of the Humerus

Elle B. K. Liagre[1] | Floriane Remy[1] | Sébastien Villotte[2,3,4] | Christopher J. Knüsel[1]

[1]PACEA UMR 5199, CNRS, Université de Bordeaux, Ministère de la Culture, Pessac, France | [2]UMR 7206 Éco-Anthropologie, CNRS, MNHN, Université Paris Cité. Musée de L'homme, Paris, France | [3]Quaternary Environments & Humans, OD Earth and History of Life, Royal Belgian Institute of Natural Sciences, Brussels, Belgium | [4]Unité de Recherches Art, Archéologie, Patrimoine, Université de Liège, Liège, Belgium

Correspondence: Elle B. K. Liagre (elle.liagre@u-bordeaux.fr)

Received: 9 December 2024 | **Revised:** 18 June 2025 | **Accepted:** 20 July 2025

Funding: This work was supported by the Université de Bordeaux, IdEx Investments for the Future program/GPR Human Past.

Keywords: 3D surface | activity-related skeletal changes | entheseal changes | humeral medial epicondyle | standardized cropping

ABSTRACT

Objectives: The medial epicondyle of the humerus has been considered particularly relevant for investigating past activity-related skeletal changes. Yet, the characterization of these skeletal changes on the humerus has been challenging. This study introduces a semi-automated cropping protocol to standardize the analysis of this anatomical region and its entheseal surfaces.

Materials and Methods: A landmark-based cropping protocol was established in 3DSlicer to capture the region of interest, identified based on anatomical literature. Before applying this protocol, mesh resolution and orientation were standardized. Repeatability and reproducibility were assessed in 20 humeri through landmark placement precision and cropped model surface area.

Results: The final cropped surface effectively encompassed the entire entheseal region. Mean landmark distances were mostly below 1 mm for intra-observer comparisons and more variable (between < 1 and 4 mm) for inter-observer comparisons. Distance-based Intraclass Correlation Coefficients (dICC) were all above 0.99. Mean percentage errors between surface areas were predominantly below 5%, with the highest value at 10.39%. Intraclass Correlation Coefficient and Lin's Correlation Coefficient values all exceeded 0.94.

Discussion: The proposed protocol offers a holistic approach to studying entheseal changes at the medial epicondyle while accommodating morphological variation. Despite some subjectivity in landmark placement, the statistical results for both landmark placement and surface area found the method's observer error to be among the lowest in comparable studies. This method provides a valuable tool for examining entheseal surface changes and morphology, with the potential, pending experimental validation, to support research on reconstructing physical activity, pathological conditions, and human evolutionary adaptation.

1 | Introduction

The medial epicondyle of the humerus serves as a key anatomical structure, anchoring the origin of the common flexors, pronator teres muscle, and medial collateral ligament (MCL) (Figure 1). These structures are responsible for wrist and finger flexion, forearm pronation, and maintaining elbow stability. Since Dutour's (1986) pioneering work, this anatomical area has been considered particularly relevant for investigating past activity-related skeletal changes (Capasso et al. 2004; Dutour 2000; Knüsel 2011; Polet et al. 2019; Varalli et al. 2020; Villotte et al. 2010). This interest stems from extensive medical research, particularly in occupational and sports medicine (e.g., Bucknor et al. 2016; Patel et al. 2014), which shows that the medial epicondyle is frequently

Summary

- A semi-automated cropping protocol was developed to standardize the analysis of the humeral medial epicondyle and its entheseal surfaces.
- Intra- and inter-observer tests showed high reliability in landmark placement and cropped surface areas.

affected by activities involving overhead throwing movements. Baseball, especially pitching, has been thoroughly studied in this context (e.g., Daruwalla et al. 2017), but other sports such as golf, tennis, and bowling may also contribute to medial epicondyle strain (Vangsness and Jobe 1991). Beyond sport-related activities, occupations requiring repetitive and forceful pronation, such as assembly line packing or hammering in carpentry, may pose similar risks (Ciccotti et al. 2004; Shiri and Viikari-Juntura 2011; Walker-Bone et al. 2012). In prehistoric contexts, comparable mechanical stresses may have resulted from activities such as slinging projectiles or ax use (Villotte and Knüsel 2014). However, bioarcheological studies encounter a significant methodological challenge: the changes observed in the medial epicondyle, particularly at the attachment of the MCL, take highly varied forms that are difficult to characterize.

The humerus has long been a focal point in bioarchaeology and biological anthropology for reconstructing past human activity. Its morphological adaptations, shaped primarily by manual loading rather than locomotion, can be analyzed through biomechanical analyses to gain insights into functional adaptations of past human populations (e.g., Scherf et al. 2016; Sládek, Ruff, et al. 2016; Trinkaus et al. 1994). Cross-sectional geometry reveals patterns of robusticity and bilateral asymmetry (e.g., Profico et al. 2021; Rhodes and Knüsel 2005; Shaw et al. 2012; Shaw and Stock 2009; Sládek, Hora, et al. 2016; Sparacello et al. 2017; Stirland 1993), while studies on structural measurements such as torsion (Churchill and Rhodes 2009; Rhodes and Churchill 2009) and internal structures such as trabecular bone organization (e.g., Perchalski et al. 2018; Scherf et al. 2016) further contribute to understanding biomechanical adaptations (Scherf et al. 2016; Sparacello et al. 2017; Trinkaus et al. 1994). Additionally, mechanical stress can induce pathological changes, particularly at entheses (Villotte et al. 2010; Villotte and Knüsel 2014).

Entheses, i.e., sites where muscles, tendons, and ligaments attach to bone, began to be systematically studied in the late 20th century to reconstruct past activity patterns (Dutour 1986; Hawkey and Merbs 1995; Kennedy 1983). Early studies focused on the qualitative recording of entheseal changes, classifying them into stages of increasing development (e.g., Hawkey and Merbs 1995; Robb 1998), but often neglected the underlying etiology. Later researchers proposed more standardized recording protocols (e.g., al-Oumaoui et al. 2004; Mariotti et al. 2004, 2007) and incorporated biomedical data in their approach (e.g., Villotte 2006). These efforts culminated in the development of the Coimbra method (Henderson 2013), which considers different types of changes, such as porosity and bone formation, reflecting the complexity of entheseal changes. While qualitative methods are straightforward and equipment-free, they are inherently subjective (Davis et al. 2013; Weiss 2015).

Quantitative methods offer a more objective way to study entheseal changes. Early efforts focused on 2D measurements of entheseal size (Churchill and Morris 1998; Stirland 1993; Wilczak 1998), but these have been criticized for capturing limited spatial information (Henderson 2013; Nolte and Wilczak 2013; Zumwalt 2005). Later approaches addressed this by recording entheseal changes three-dimensionally. Several studies have focused on recording entheseal profiles (Feuerriegel 2016; Henderson 2013; Zumwalt 2005), but as 3D techniques became more accessible, fully three-dimensional approaches were embraced. This enabled the exploration of different aspects of entheses, such as 3D surface area as a measure of entheseal size and surface topography (Bucchi et al. 2020;

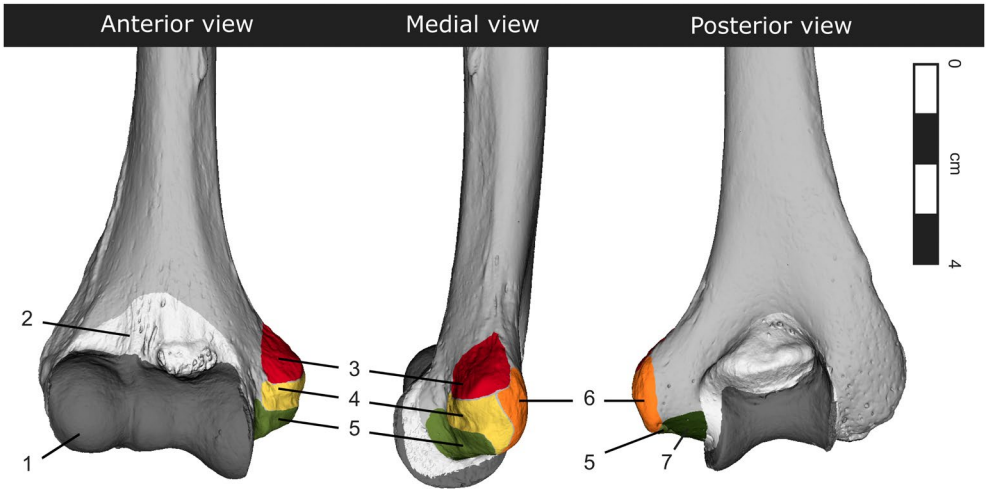

FIGURE 1 | Anatomical representation of the entheseal attachments at the medial epicondyle on a 3D model of a right humerus from the Scientific and Educational Collection of PACEA, University of Bordeaux (TP 67) (after Buck et al. 2010; Fuss 1991; Ikezu et al. 2020; Labott et al. 2018; Netter 2019). The indicated areas are (1) the articular cartilage, (2) the joint capsule, (3) the attachment site of the pronator teres muscle, (4) the attachment site of the common flexor tendon (anterior aspect), (5) the attachment site of the medial collateral ligament (anterior bundle), (6) the attachment site of the common flexor tendon (posterior aspect), (7) the attachment site of the medial collateral ligament (posterior bundle).

Karakostis and Lorenzo 2016; Noldner and Edgar 2013; Nolte and Wilczak 2013; Pany et al. 2008; Williams-Hatala et al. 2016), entheseal shape (Abdel Fatah et al. 2012; Casado et al. 2019; Karakostis et al. 2018), and topographical analyses to characterize surface changes (Karakostis 2025; Nikita et al. 2019; Wallace et al. 2017).

However, these approaches also introduce new challenges. The relationship between measurements and their biological significance is complex, and sensitivity to 3D resolution and taphonomic damage—although the latter is also problematical for qualitative methods—tends to pose great challenges to quantitative approaches. Moreover, these approaches often contain a level of subjectivity in delineating entheses, particularly in complex regions like the humeral medial epicondyle. At this location, multiple structures, including the origins of the common flexor tendon, the pronator teres muscle, and MCL are situated adjacently, making it difficult to distinguish between them. Existing methods generally focus on the common flexor origin (Hawkey and Merbs 1995; Ieng et al. 2024; Robb 1998; Villotte 2006), and less frequently on the pronator teres origin (Feuerriegel 2016), with only Varalli et al. (2020) attempting to include the area of the MCL.

This lack of comprehensive methods is particularly significant because the medial epicondyle, and in particular the attachment site of the MCL, has potential as an indicator of activity. The region experiences significant stress when performing activities involving overhead throwing movements (e.g., Bucknor et al. 2016; Nakanishi et al. 1996; Patel et al. 2014), which can lead to pathological surface alterations (Polet et al. 2019). However, these alterations can take highly varied forms that are difficult to characterize. The current study aims to address this by proposing a standardized method for cropping the medial epicondyle and its entheses. This will smooth the way for future quantitative analyses of this region and ensure consistency among studies.

2 | Materials and Methods

2.1 | Materials

The Scientific and Educational Collection of PACEA (De la Préhistoire à l'Actuel: Culture, Environnement, et Anthropologie) Laboratory (UMR-5199, Université de Bordeaux) served as the basis for constructing the protocol and assessing its repeatability and reproducibility. Assembled in the 1980s, this collection includes 102 human humeri, primarily from post-medieval archeological sites in France's Gironde region. A study sample of 20 humeri was selected based on a previous study by Bourreau (2021), which aimed to capture a broad range of morphological variation in the medial epicondyle region. From the 102 humeri, specimens from physiologically mature adults with well-preserved medial epicondyles were retained ($N = 48$), followed by ranking the remaining humeri based on the intensity of entheseal changes to select a representative sample of 20. Within this selection, three humeri with damaged trochleae were excluded and replaced with the best-preserved alternatives. Although the sample aimed for an equal distribution of right and left humeri, the final selection included 11 left and 9 right specimens due to preservation constraints. Additional details about the study sample, including laterality, degenerative changes, preservation, and size, are available in S1.

All selected humeri were digitized using an Artec Space Spider 3D surface scanner with the accompanying *Artec Studio 15 Professional* software (Artec 3D Inc., Luxembourg). The scanner was moved manually around each humerus, requiring four to six scans at a speed of eight frames per second. After scanning, the base of each model was manually removed using the eraser tool, and the scans were automatically aligned. Global registration was performed at a key-frame ratio of 0.1 mm, while frames exceeding 0.1 mm error threshold were removed. The next steps included outlier removal with a 3D resolution of 0.1 mm, sharp fusion at the same resolution, small-object filtering ("All except largest" option), and mesh simplification using the "Shape deviation" option with a maximum deviation of 0.01 mm. The default settings were used when parameters were not specified. The final 3D models were named "Model" followed by a number from 1 to 20, and then exported in .obj format.

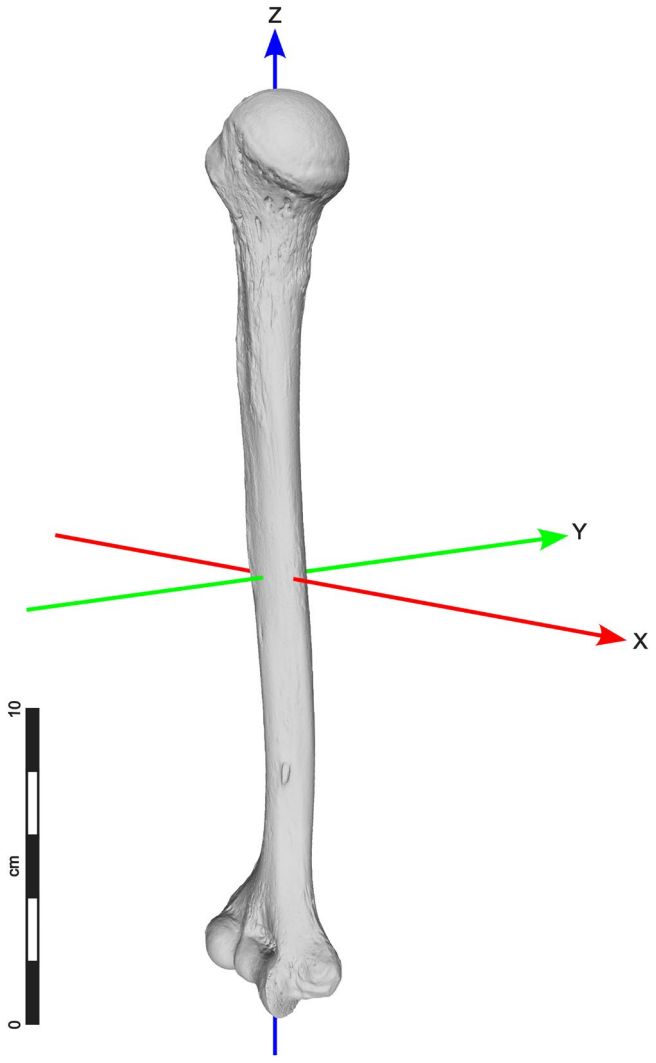

FIGURE 2 | 3D model of a right humerus oriented in anatomical position.

2.2 | Pre-Processing of 3D Models

3D models were standardized in resolution and orientation to ensure reproducibility and facilitate comparisons. Mesh resolution was set at 22 faces/mm^2, balancing preservation of topology and simplification. Retriangulation and simplification were performed automatically using the open-source software MeshLab (Cignoni et al. 2008). Anatomical alignment was automated using 3DSlicer's FastModelAlign module (Fedorov et al. 2012), with reference to an oriented humerus model (Figure 2), available in the MorphoSource 3D repository. Technical details of these procedures, including their automation, are provided in Supporting Information S2–S5.

2.3 | The Cropping Protocol

This study aimed to develop a standardized methodology for cropping the entheseal surfaces on the medial epicondyle, with a focus on the MCL. However, the common flexor origin and the MCL share an intimate relationship, creating a single complex of fibrocartilaginous entheses with indistinct boundaries between them (Milz et al. 2004). This structure can be described as a "multi-enthesis organ," where adjacent tendons or ligaments share an attachment site (Benjamin et al. 2006), which helps dissipate stress over a broader area. Therefore, the entire entheseal surface was taken into account. To define the region of interest, a thorough review of the anatomical literature was conducted (Buck et al. 2010; Fuss 1991; Ikezu et al. 2020; Labott et al. 2018; Netter 2019), and the findings were illustrated on a three-dimensional model (Figure 1).

Given that the area lacks distinct anatomical boundaries, a landmark-based approach was proposed to effectively capture the variability of the medial epicondyle and its associated entheses. Six landmarks were used to guide the cropping process, as defined by Horbaly (2023) (following Tallman (2013)) and Vance and Steyn (2013) (Figure 3 and Table 1). These landmarks were selected for their anatomical relevance, as they represent key points that define the boundaries of the entheseal region and reflect the natural contours of the medial epicondyle. Landmarks 1 to 3 were used to define a plane that separated the entire medial epicondyle from the humerus. This initial crop was then refined by removing the medial trochlear border, using landmarks 2 through 6 placed along the primary curve of the border. The curve was resampled to fully encompass the border, using a buffer zone to exclude most of the trochlea.

The base size of the buffer zone was determined empirically, defined as the diameter (d) of the circumscribed circle of Landmarks 4 to 6, divided by 6, to account for variations in individual humerus size. Given that the semilunar area is larger anteriorly, this measure was adjusted to d/4 for the curve segment between Landmarks 4 and 5. The spacing between points for resampling was set to a slightly smaller value than that of the buffer zone—that is, d/8—to ensure sufficient border coverage. This process yielded two parts: the remainder of the trochlea and the isolated medial epicondyle, with the latter retained for further analysis.

A Python script was developed to automate the placement of landmarks 4 to 6 based on the bounding box of the model and to execute the entire protocol as a batch process. Technical details and scripts can be found in Supporting Information S2, S6, and S7. The cropping script works on right-sided humeri only due to orientation requirements; when applied to a left humerus, the selection of the cropped model is reversed. Left humeri that had been mirrored for alignment and cropping can be reverted to their original anatomical orientation using the script provided (S4).

2.4 | Repeatability and Reproducibility

The semi-automatic protocol requires limited user input to place the landmarks. This introduces a degree of subjectivity. To address this, reliability was assessed on two levels: (1) the precision of landmark placement, and (2) the consistency of the resulting cropped surface areas. Landmark data were collected from the sample for all landmarks specified in the proposed protocol (Table 1). Of these, only three (LM1-3, that is, the medialmost point of the olecranon fossa and the anterior and posterior extremes of the medial margin/ridge of the trochlea) required manual placement and were therefore further analyzed for reliability.

The first author (E.L.), experienced with humeral specimens and the 3D Slicer software, collected data across five sessions, each at least 5 days apart to mitigate learning effects. A second observer (F.R.), familiar with general landmarking methods but inexperienced with both humeri and the software, conducted a single data-collection session following written instructions. Both observers were blinded to prior measurements to reduce bias. Additionally, the sequence of models and landmark placements were randomized to control for order effects, learning biases, and fatigue. After pre-processing, the landmark coordinates were transformed and exported as .fscv files, which permitted visual inspection of the model and landmarks to identify random errors, such as an incorrectly numbered landmark. Such errors were manually corrected.

Reliability assessments were performed using R (v4.3.2; R Core Team 2023), RStudio (v2024.04.1.748; Posit team 2024) and the packages "GUniFrac" (v1.8, Chen et al. 2023), "irr" (v0.84.1, Gamer et al. 2012) and "DescTools" (v0.99.57, Signorell 2024). Landmark placement precision was assessed on a landmark-by-landmark basis to focus on individual precision rather than the entire configuration (Corner et al. 1992; Hirst et al. 2018; Ross and Williams 2008; Von Cramon-Taubadel et al. 2007). Given that the models were in a constant frame of reference, direct comparisons were performed by calculating Euclidean distances between corresponding points. To accommodate the non-normal distribution of coordinates and their non-monotonic relationships, a distance-based Intraclass Correlation Coefficient (dICC) was used to assess agreement within and between observers (Chen and Zhang 2022). Standard error estimates were derived from bootstrapping. Intraclass correlation coefficients (ICC) values range from 0 to 1, with a value of 1 indicating complete agreement. While there are no universal thresholds for acceptable ICC values, Koo and Li (2016) provided general guidelines for interpreting traditional ICC values: poor (<0.5), moderate ($0.5<x<0.75$), good ($0.75<x<0.9$), and excellent reliability

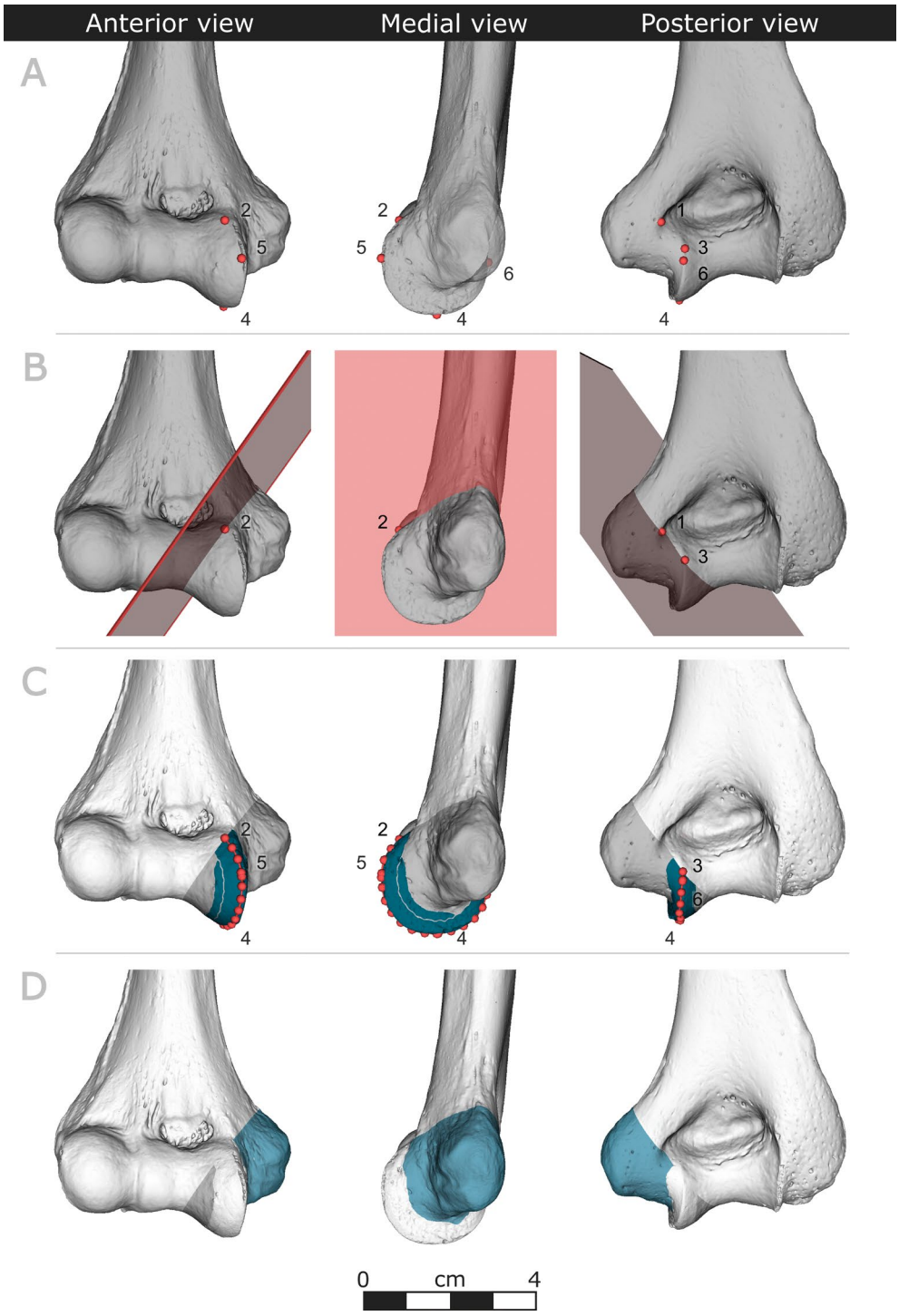

FIGURE 3 | Illustration of the cropping protocol in anterior, medial, and posterior views. (A) Designation of landmarks. (B) The 3D model was cropped using a plane defined by Landmarks 1–3. (C) Excision of the trochlear border based on Landmarks 2–6; the white line marks the boundary between the two buffer zones. (D) Resulting crop of the medial epicondyle (highlighted in blue).

(> 0.9). These guidelines, however, should be interpreted cautiously in the context of dICC results.

The second part of the analysis assessed protocol reliability by comparing the 3D surface areas of cropped models (Schlager 2017). The cropping procedure used the collected landmarks and followed the described script. Descriptive statistics and percentage errors were calculated to compare each pair of measurements. Percentage error (PE) was defined as the absolute difference between two values, divided by their mean, and then multiplied by 100. Correlation coefficients were used to analyze repeatability and reproducibility when normal distribution assumptions were met. Agreement within and between observers was assessed using the ICC (Gamer et al. 2012) as well as Lin's concordance correlation coefficient (CCC) through pairwise comparisons

(Lin 1989; Signorell 2024). The ICC, commonly used in similar studies, permits comparisons with the existing literature. Lin's CCC complements the ICC by measuring precision and accuracy, making it suitable for assessing agreement between continuous variables. As with the ICC, a value of 1 for the CCC indicates complete agreement, whereas values can range down to −1, representing systematic disagreement. Although no universally accepted thresholds exist for CCC interpretation, Altman (1999) recommended interpreting values similarly to other correlation coefficients (e.g., values above 0.8 indicate excellent agreement, and those below 0.2 are considered poor). Some fields use more conservative benchmarks, considering values below 0.9 as poor agreement (McBride 2005).

TABLE 1 | Overview of the landmarks selected for cropping.

Landmark number	Anatomical region	Landmark definition
1	Olecranon fossa	Medial-most point of the olecranon fossa
2	Trochlea	Viewed anteriorly: proximomedial extreme of the trochlea
3	Trochlea	Viewed posteriorly: proximomedial extreme of the trochlea
4	Trochlea	Distomedial extreme of the trochlea
5	Trochlea	Viewed medially: Anterior extreme of the medial margin/ridge of the trochlea
6	Trochlea	Viewed medially: Posterior extreme of the medial margin/ridge of the trochlea

Note: Landmarks 2–4 were adapted from Horbaly (2023) (after Tallman (2013)), whereas landmarks 1, 5, and 6 were loosely adapted from Vance and Steyn (2013).

3 | Results

3.1 | Assessment of the Cropped Model

The final cropped surface effectively encompassed the entire entheseal region, as identified in the anatomical literature (Figure 4, see S8 for the results of the full study sample). On the anterior side, the boundaries of the cropped surface align closely with the general contours of the region of interest, with an additional margin of a few millimeters. On the posterior side, the entheseal surface forms a right angle, resulting in a triangular area as a cropping surplus beyond the entheseal surface. This surplus reflected the geometric nature of the cropping process and its interaction with the anatomical shape of the model.

3.2 | Reliability of Landmark Placement

Visual inspection of the collected landmarks revealed several mislabeled points, which were subsequently corrected manually. One data point from Observer 2 was excluded from the analysis because of a significant error in placement, where Landmark 1 was placed anteriorly instead of posteriorly. The Euclidean distance calculations for landmark placement are presented in Figure 5, and further detailed in Supporting Information S9.

For Observer 1, the overall mean Euclidean distances across the three landmarks remained consistently below 1 mm. Landmark 2 showed slightly larger distances, primarily influenced by the higher distance values for models 6 and 9. These models also demonstrated the largest distances for Landmarks 1 and 3. Nonetheless, the remaining models had mean distances of less than or approximately 1 mm. When comparing the measurements of Observer 1 to those of Observer 2, the mean distances generally increased. For Landmark 1, most values remained at or below 1 mm, while the majority of distances for Landmark 2 remained below the threshold of 1.5 mm, with the higher distances again attributed to models 6 and 9. Landmark 3 showed the greatest variability between the observers, with some models exceeding 3 mm. Despite these elevated values, the low standard deviations (e.g., ±0.2 mm for many points) suggest that differences in placement were systematic rather than random.

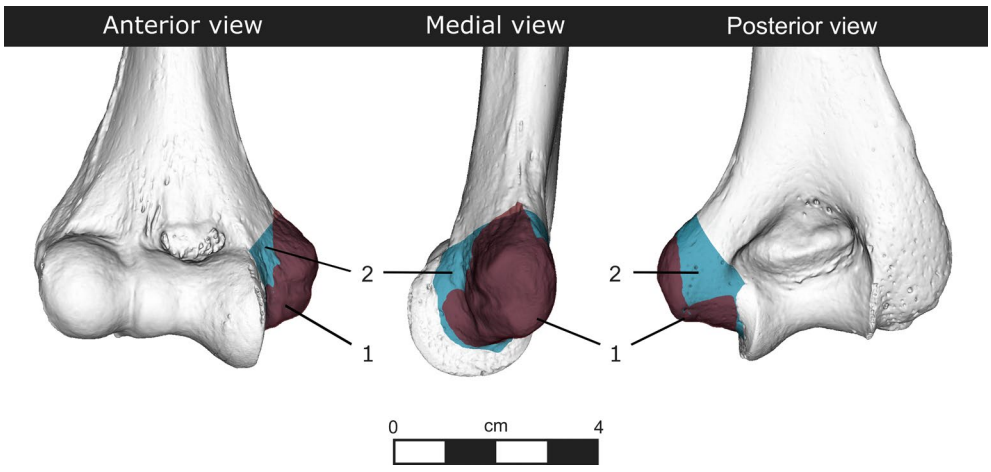

FIGURE 4 | Visual comparison of the anatomical representation of entheseal attachments at the medial epicondyle (1) and the final 3D cropped model (2), shown from anterior, medial, and posterior perspectives.

The distance-based ICC analysis yielded values of 0.99 for both intra- and inter-observer comparisons (Table 2, further detailed in S9 Table S2.1), indicating excellent reliability. The confidence intervals for the intra-observer tests (0.97–1.00) were slightly narrower than those for the inter-observer tests (0.95–1.00), reflecting a higher consistency in repeated measures conducted by Observer 1.

3.3 | Reliability of Resulting Cropped Model

When examining the cropped surface areas, the majority of the mean PE results were below 5%, with nearly all values falling under 10% for both the intra- and inter-observer comparisons (Table 3, further detailed in S10 Tables S2.1 and S2.2). Overall, the mean PE was 3.31% (±2.50%) for intra-observer comparisons and 4.82% (±3.45%) for inter-observer comparisons. These results indicate that the measurements tended to be slightly more consistent when taken by the same observer than when taken by different observers. Most models exhibited standard deviations below 4%, reflecting consistent error measurements. The highest intra-observer variability was observed in Model 9, with a mean PE of 6.24%. However, specific comparisons between measurement series for this model showed even greater variability, with some values reaching up to 11.98%. For inter-observer comparisons, the greatest variability was found in Model 11, with a mean PE of 10.39% and a peak value of 13.51%.

As the Shapiro–Wilk test did not show evidence of non-normality ($p > 0.05$) (see S10 Table S3.1), correlation coefficients were calculated. All values exceeded 0.94, supporting the agreement between measurement series. The ICC value for

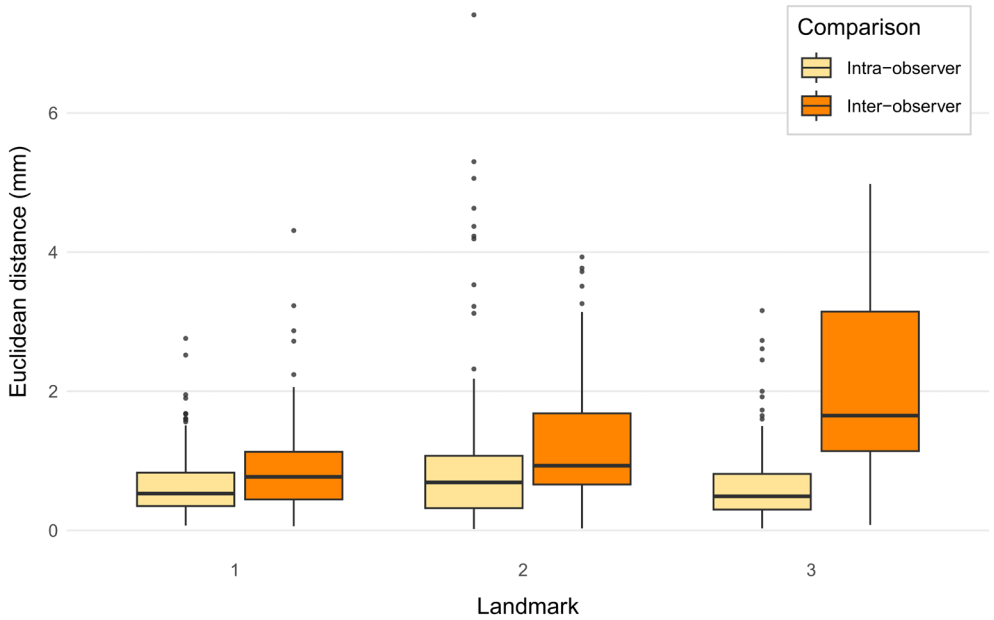

FIGURE 5 | Summary boxplots of Euclidean distances between landmarks. Intra-observer distances represent the distances between all combinations of corresponding points across five sets placed by the same observer ($N = 10$). Inter-observer distances compare the distances between the points placed by Observer 2 and each of the corresponding points in the five sets placed by Observer 1 ($N = 5$). The detailed results are available in S9 Tables S1.1 and S1.2.

TABLE 2 | Distance-based intraclass correlation coefficient (dICC) results.

	Distance-based intraclass correlation coefficient	Systematic error	95% Confidence interval	
			Lower bound	Upper bound
Intra-observer				
Landmark 1	0.999	0.014	0.971	1.000
Landmark 2	0.998	0.012	0.972	1.000
Landmark 3	0.999	0.010	0.979	1.000
Inter-observer				
Landmark 1	0.999	0.024	0.953	1.000
Landmark 2	0.998	0.019	0.960	1.000
Landmark 3	0.992	0.019	0.955	1.000

Note: The ICC was calculated with 100,000 bootstrap iterations. The intra-observer results included all five observation sets from Observer 1. Inter-observer results compare the average of Observer's sets with the single set from Observer 2. Comparisons between each set of Observer 1 and Observer 2 are detailed in S9 Table S2.1.

TABLE 3 | Summary of the percentage of error (PE) for 3D surface area (mm^2).

	Intra-observer		Inter-observer	
Name	Mean PE (%)	Standard deviation of the mean PE (%)	Mean PE (%)	Standard deviation of the mean PE (%)
Model 1	3.48	2.01	4.36	2.80
Model 2	1.80	1.44	1.56	1.48
Model 3	4.18	2.98	5.51	3.57
Model 4	1.81	1.31	1.29	1.53
Model 5	2.24	1.51	5.53	1.88
Model 6	2.82	1.70	7.83	2.29
Model 7	2.14	1.32	1.92	1.75
Model 8	4.25	2.77	7.57	3.53
Model 9	6.24	3.49	8.05	4.99
Model 10	1.98	1.16	3.75	1.60
Model 11	4.13	2.79	10.39	3.46
Model 12	4.12	2.42	5.15	3.33
Model 13	4.83	3.13	5.29	4.01
Model 14	4.23	2.32	3.76	2.76
Model 15	1.96	1.23	2.29	1.61
Model 16	2.47	1.96	4.97	2.19
Model 17	2.03	1.13	3.94	1.62
Model 18	4.77	3.04	4.89	3.87
Model 19	4.92	2.89	3.60	1.86
Model 20	1.83	1.19	—	—
All models	3.31	2.50	4.82	3.45

Note: Intra-observer results represent the errors between all combinations of corresponding measurements ($N = 10$) across all sets placed by Observer 1 (Sets 1A to 1E). The inter-observer results show the PE between the measurements by Observer 2 (Set 2A) and each of the corresponding datasets of Observer 1 ($N = 5$). The detailed results are available in S10 Tables S2.1 and S2.2.

the intra-observer test was 0.98, while for the inter-observer tests they ranged between 0.95 and 0.98 (Table 4). Similarly, Lin's CCC values ranged from 0.96 to 0.99 for the intra-observer assessments, while the inter-observer assessments showed slightly more variation, ranging from 0.95 to 0.98 (Figure 6, further detailed in S10 Table S3.2 and Figures S3.1 and S3.2).

4 | Discussion

A cropping protocol was established to extract the area of interest, yielding generally positive results. The final cropped surface encompassed the entire entheseal region of the medial epicondyle, including an additional margin. The presence of a margin can be considered an advantage, as the boundaries of the entheseal surface are not always easy to delineate. It is important to note that, due to inherent anatomical variability and the lack of direct soft tissue data, especially in archeological samples, our protocol captures a generalized entheseal region based on anatomical literature, rather than the exact individual tendon footprints. Other studies have addressed this challenge using different approaches. For instance, the Validated Entheses-based Reconstruction of Activity (V.E.R.A.) method delineates entheses based on the surface elevation using imaging filters (Karakostis and Harvati 2021; Karakostis and Lorenzo 2016). Consequently, the traced area does not align precisely with the footprints of the entheses, nor is it intended to. Ieng et al. (2024) applied this protocol to the medial epicondyle of the humerus. When compared to the anatomical literature (e.g., Figure 1), their approach primarily captures the common flexor origin while also including parts of the pronator teres muscle and MCL area, leaving some parts of the entheseal surface unaccounted for. In contrast, our protocol aims to encompass the full entheseal surface of the medial epicondyle, providing a more comprehensive representation for further analysis.

Moreover, multiple studies applying the V.E.R.A. method excluded individuals with osteophytic or osteolytic lesions, generally larger than 1 mm, from their samples (Bousquié et al. 2022; Karakostis and Harvati 2021; Karakostis and Hotz 2024; Karakostis and Lorenzo 2016). This criterion, based on Benjamin et al. (2000), was intended to eliminate entheses affected by degenerative, inflammatory, or metabolic factors, ensuring a stronger link to mechanical loading in the remaining sample. While this approach helps control for potential pathological influences on entheseal morphology, it also limits the range of surface variations considered. In contrast, the cropping method presented here did not systematically exclude individuals based on lesion size but allows for a certain degree of variation. This suggests that, up to a certain threshold, the protocol remains reliable in terms of measurement repeatability and reproducibility, even in the presence of entheseal alterations. Depending on their research question, researchers may choose to exclude specimens with indications of pathology, as done in previous studies, or include them to assess their impact on measurements and on the inferred activity reconstructions. Although experimental validation is necessary to determine if incorporation of these variations provides meaningful insights in entheseal-based reconstructions of physical activity, this cropping method offers a framework to explore the relationship between physical activity and entheseal changes. Other studies (e.g., Castro et al. 2022; Turcotte et al. 2022) have shown reliable links between entheseal morphology and activity under controlled conditions. While not validated here, the current protocol could be tested similarly in future research.

Overall, the approach presented in this article offers a more holistic perspective to the study of entheses at the medial epicondyle, as it captures all relevant entheseal surfaces, effectively representing the complete "enthesis organ".

A notable strength of the protocol is its flexibility to account for individual morphological variation through the use of

TABLE 4 | Results of the intraclass correlation coefficient (ICC) calculation for the 3D surface area using the single-rating, absolute agreement, 2-way random-effects model.

		95% Confidence interval		*F* test with true value 0			
Observer and observation sets	**ICC**	**Lower bound**	**Upper bound**	**Value**	**df1**	**df2**	**Sig.**
Intra-observer ($N = 20$)							
1A, 1B, 1C, 1D & 1E	0.977	0.957	0.990	230.390	19	74	< 0.0001
Inter-observer ($N = 19$)							
1 & 2A	0.966	0.713	0.991	115.469	18	4	< 0.0001
1A & 2A	0.951	0.753	0.985	64.345	18	5	< 0.0001
1B & 2A	0.951	0.501	0.987	90.593	18	3	0.002
1C & 2A	0.979	0.926	0.993	126.370	18	9	< 0.0001
1D & 2A	0.951	0.811	0.983	55.645	18	8	< 0.0001
1E & 2A	0.958	0.703	0.988	87.539	18	4	< 0.0001

Note: For the intra-observer comparisons, which use the observation sets of Observer 1 (Sets 1A to 1E), the sample size is $N = 20$. For the inter-observer comparisons, which involve the observation sets of Observer 1, their average (Set 1) and Observer 2 (Set 2A), the sample size is $N = 19$.

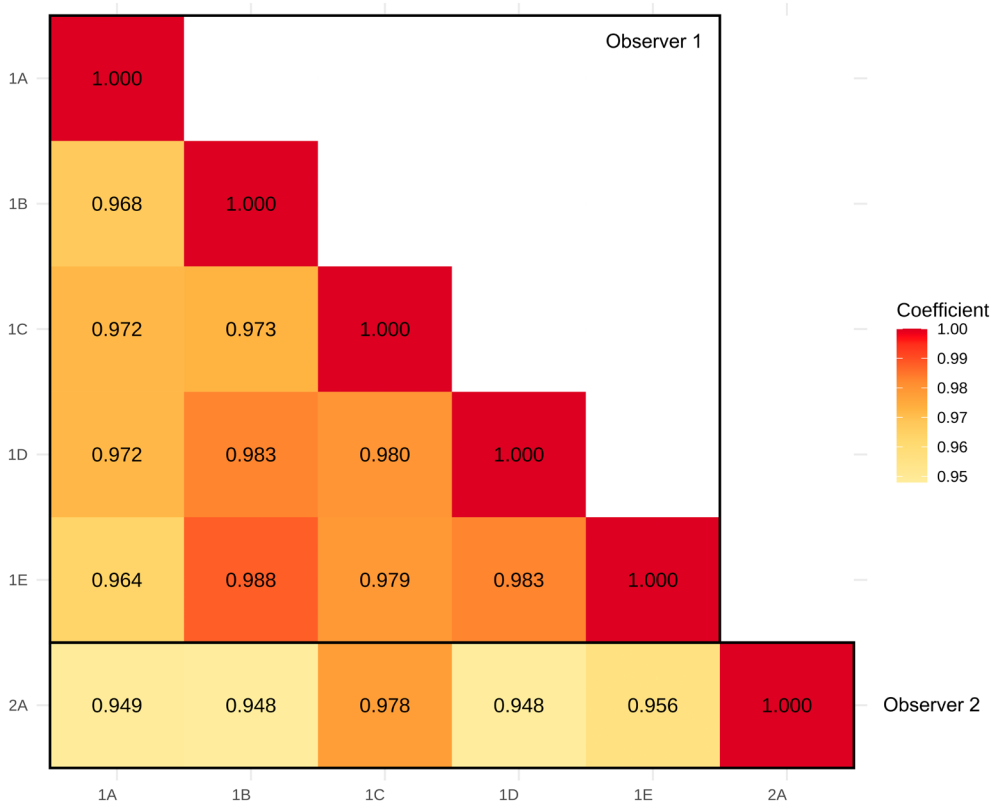

FIGURE 6 | Overview matrix of Lin's Concordance Correlation Coefficients (CCC). This matrix displays pairwise comparisons of CCC values for 3D surface area measurements of the cropped models. Intra-observer coefficients were calculated using data from 20 individuals across all sets of Observer 1 (1A to 1E), while the inter-observer analysis involved 19 individuals, comparing Observer 2's results (2A) with each measurement series from Observer 1. The detailed results are available in S10 Table S3.2.

landmarks and measurements. However, similar to other 3D methods for assessing entheses, the cropping protocol retains a degree of subjectivity. Overall, intra-observer variability was low, with most Euclidean distances below 1 mm, indicating high precision in repeated measurements by a single observer. The inter-observer results, while generally exhibiting larger distances, still suggest reasonable consistency, particularly for Landmarks 1 and 2. Outliers identified within and between observers highlight cases where landmark placement might be inherently more challenging. Upon closer inspection of the relevant models, the highest values for Landmark 1 corresponded to individuals with a less pronounced transition

between the olecranon fossa and medial epicondyle, making it more difficult to place the landmark accurately. Even with this variability, the distances for this landmark are generally low (0.90 ± 0.59 mm), and landmark placement can be considered stable. Regarding Landmarks 2 and 3, the highest values corresponded mostly with individuals in whom the interpretation of the "trochlear border" could be considered ambiguous. In these cases, there was a distortion of the articular margin, expressed as a raised and/or thickened rim, or the rim did not correspond to the articular margin. For Landmark 3, the results indicate higher distances in inter-observer comparisons (2.12 ± 1.27 mm), but in many instances, the standard deviations remain low (< 0.30 mm). This suggests that Observer 2's measurements consistently deviated from the stable measurements of Observer 1. This discrepancy could be interpreted as the result of the difference in experience level between the observers. Potential strategies to mitigate this variability include training observers to become more familiar with the biological landmarks and the variability in their expressions prior to performing the formal cropping, as demonstrated in several studies (e.g., Shearer et al. 2017). Additionally, including the model texture and/or improving the lighting to observe the bone surface more clearly could improve precision.

The findings of this study appear to be consistent with existing literature evaluating 3D landmark placement precision through Euclidean distance. For example, Olszewski et al. (2008) reported mean intra-observer distances of less than 1.5 mm and inter-observer distances of ≤ 2 mm for cranial landmarks placed on surface renderings derived from CT scans. Similarly, Corron et al. (2022) examined agreement and error rates in 3D virtual non-adult crania and found that landmark placement variation was generally within a 5 mm range. For dental landmarks, precision tended to be higher, with most permanent and deciduous cervical landmarks placed within a 2 mm range for both observers. This is likely due to the smaller, more clearly defined surfaces of the teeth, which permit clearer identification of landmarks. No similar studies for the humerus were identified in the current literature. While the results in this study align with prior research, establishing an appropriate threshold for precision remains challenging (cf. Hirst et al. 2018). Such thresholds depend not only on the scale of the study object (e.g., cranium vs. teeth) and the nature of the selected landmarks but also on the required level of measurement precision for a specific study.

The distance-based ICC provides an additional perspective on landmark placement. When interpreted similarly to traditional ICC metrics, these results indicate a high level of agreement in landmark placement (dICC > 0.99), both within and between observers. However, the acceptable level of variation ultimately depends on the intended application and the potential impact of this variability on the study results, which in this study is the cropping of the medial epicondyle.

Differences between the cropped models were assessed by comparing their 3D surface areas. The percentages of error predominantly fell below 5%, and almost all fell under 10%. As for the landmarks, inter-observer comparisons generally had higher mean values, though this was not consistent across all models. Notably, the models identified as having outliers in landmark placements did not always correspond to those with high percentage errors in surface areas. This suggests that other factors, such as morphological variation among models, could also influence the results. Overall, variation within and between observers appears limited, a conclusion supported by the correlation coefficients (all above 0.94). Following the guidelines of Koo and Li (2016) for ICC interpretation, excellent reliability was observed for both intra- and inter-observer tests. Lin's CCC results mirrored these findings, further reinforcing the idea that any systematic bias present is likely minimal. Although interpretation guidelines for this coefficient vary, even the more conservative standards suggest a substantial strength of agreement across all observation sets.

Several studies have explored the 3D analysis of entheses. Nolte and Wilczak (2013) proposed a method delineating entheses on dry bone, followed by scanning and measurement, reporting mean intra-observer error ranging from 12.58% to 16.65% for a sample of 25 radii. Noldner and Edgar (2013) applied a similar method to seven entheses on upper limb elements, finding intra-observer error rates between 10% and 15% ($N = 12$), comparable to those reported by Nolte and Wilczak (2013). In contrast, Williams-Hatala et al. (2016) performed delineation directly on 3D models of metacarpals ($N = 5$), with mean intra- and inter-observer errors of 2.6% and 4.0%, respectively. Using the V.E.R.A. method, Ieng et al. (2024) reported mean intra-observer errors ranging from 1.83% to 3.23% for four entheses/entheseal groups on the humerus ($N = 23$), including the common flexor origin, although their calculation method differed slightly. Other studies employing the V.E.R.A. protocol to analyze hand entheses in humans and hominids have reported intra-observer percentage errors from 0.09% to 4.80% ($N = 5$ or 6), albeit also calculated with slight methodological differences (Kunze et al. 2024, 2022). In this context, the mean intra- and inter-observer errors in the present study (3.31% and 4.82%, respectively) fall within the lower range of observer errors.

Previous research utilizing the V.E.R.A. protocol has also reported Lin's CCC values for entheseal surfaces, with intra-observer values ranging from 0.88 to 0.99 for human and hominin hand entheses ($N = 5$ or 6) (Bousquié et al. 2022; Kunze et al. 2024). For the humerus, Ieng et al. (2024) reported intra-observer Lin's CCC values between 0.94 and 0.97 ($N = 23$) and inter-observer values between 0.87 and 0.99 ($N = 5$ or 7). Among these studies, only Ieng et al. (2024) calculated ICC values, which were between 0.97 and 0.99 for the inter-observer comparisons. It is worth noting that the limited sample size of some of the mentioned studies ($N = 5$–7) may have influenced the correlation coefficient, potentially reducing the ability to accurately detect true agreement levels and resulting in broader confidence intervals, which were not provided in the studies. Nonetheless, numerous studies on the V.E.R.A. protocol, including the original larger-sample study by Karakostis and Lorenzo (2016) ($N = 50$), have consistently demonstrated high measurement repeatability across different observers from diverse institutions, species (primate and laboratory), long bones, and entheses (Bousquié et al. 2022; Castro et al. 2022; Kunze et al. 2022, 2024). When comparing these findings with those of the present study (intra-observer: Lin's CCC 0.96–0.99, ICC 0.98; inter-observer: 0.95–0.98 for both Lin's CCC and ICC), the results

appear broadly similar, although the larger sample size may lend additional robustness to the findings of the current study.

4.1 | Limitations

This technique is not without limitations. The time and cost of 3D data acquisition may restrict its accessibility. Nevertheless, the ability to reuse 3D data and preserve osteological collections offers valuable opportunities for long-term research and data sharing. The protocol emphasizes accessibility by using open-source software for data processing, and with automated scripts and some familiarity with these tools, the processing time can be reduced to less than a minute per model. This efficiency makes it more feasible for broader research use despite initial time investments.

The subjectivity in the placement of landmarks remains a concern as it can affect the consistency of results. Yet, observer tests indicate that variation in landmark placement generally falls within acceptable ranges, with 3D surface area variation falling within the lower range in comparable studies. Targeted training could further minimize variability, as has been demonstrated in other studies (e.g., Shearer et al. 2017).

Pathological lesions may introduce additional variability. While lesions on the medial epicondyle itself generally do not affect the cropping process, severe changes in the distal articular surface could complicate manual landmark placement. Specifically, marginal lipping or loss of morphology in the distal articular surface could make the anatomical landmarks less distinct, thus reducing the accuracy of placement. However, our study included humeri with minor degenerative changes, and these did not correspond to the models with the lowest landmark reliability. That said, the extent of variability in more severe cases remains to be fully explored.

The condition of the cortical bone surface, which can degrade post-mortem, presents another challenge. Limited preservation of skeletal elements, especially the trochlear border that serves as a reference point, can pose difficulties. This issue could be addressed through reconstruction techniques, such as scaling other well-preserved medial epicondyles to create a reference model or using software for reconstructing missing elements, thus maintaining study integrity (e.g., Gunz et al. 2009; Jani et al. 2020; Lautenschlager 2016).

Lastly, the method includes a margin around the entheseal surface, which makes it unsuitable for using it directly as the 3D entheseal surface area. Notably, the larger margin on the posterior side of the crop remains a concern, as it was not possible to objectively decrease this margin at this stage. Nevertheless, given the typically minimal changes in this region, this is considered a minor shortcoming. Despite this, the approach does ensure that the entire medial epicondyle is included, even in cases where entheseal margins may be hard to distinguish. At the same time, the increased complexity of the analyzed surface poses challenges in interpreting the relationships between observed changes and underlying biomechanical processes. Future research could refine the approach to enable more detailed analyses of the individual entheseal surfaces, although a more comprehensive understanding of the footprint of the different entheses is needed.

5 | Conclusions

This study presents a semi-automated method for acquiring surface models of the medial epicondyle of the human humerus that is both repeatable and reproducible. By capturing the entire entheseal surface, the technique offers a new approach for characterizing the highly varied surface alterations in this area, which has been challenging to date. The inclusion of the entire entheseal surface enables a detailed analysis of surface changes and morphology, providing a foundation for more advanced quantitative studies such as 3D topographical analysis. Consistent identification of the region of interest is ensured by the protocol's use of anatomical landmarks to guide cropping, with observer testing showing low error rates. This makes it one of the more repeatable and reproducible approaches among comparable studies. Further improvement may be possible through targeted observer training or user-guided automated landmarking methods (e.g., Porto et al. 2021). Moreover, the method could be improved by reducing the posterior margin of the cropped area and by applying the proposed strategies to deal with taphonomically damaged surfaces.

Despite these limitations, the proposed cropping method can be considered a valuable tool for analyzing the complex entheseal surface of the humeral medial epicondyle. It paves the way for future analyses of this region and guarantees consistency between studies. While this method holds promise for exploring the relationship between entheses, pathology, and physical activity, as well as placing these findings within a broader context, such as the biomechanics of the elbow and upper limb (e.g., Ibáñez-Gimeno et al. 2013), its potential applications in activity reconstruction remain contingent on experimental validation under controlled conditions. Future research could also focus on adapting the method to other complex anatomical regions, such as the lateral epicondyle of the humerus, as well as testing its applicability to other primate species. As such, this method can serve as a stepping-stone to a wider range of research applications, from investigating palaeopathological conditions affecting entheses to making broad comparisons of this anatomical region in living and fossil primates, and thereby contribute to our understanding of human adaptation, variability, and evolution.

Author Contributions

Elle B. K. Liagre: conceptualization (lead), data curation (lead), formal analysis (lead), investigation (lead), methodology (lead), software (lead), visualization (lead), writing – original draft (lead), writing – review and editing (lead). **Floriane Remy:** data curation (equal), writing – review and editing (supporting). **Sébastien Villotte:** conceptualization (equal), formal analysis (supporting), funding acquisition (equal), investigation (equal), methodology (equal), supervision (equal), writing – original draft (equal), writing – review and editing (equal). **Christopher J. Knüsel:** conceptualization (equal), formal analysis (supporting), funding acquisition (equal), investigation (equal), methodology (equal), supervision (equal), writing – original draft (supporting), writing – review and editing (equal).

Acknowledgments

Elle B. K. Liagre would like to thank the Slicer community for their valuable advice and assistance, which contributed to the successful completion of this work. This study received financial support from the French government in the framework of the University of Bordeaux's IdEx "Investments for the Future" program/GPR "Human Past".

Ethics Statement

The authors were granted approval for this study by Maryelle Bessou, Curator of the Scientific and Educational Collection of the PACEA (De la Préhistoire à l'Actuel: Culture, Environnement, et Anthropologie Unité Mixte de Recherche (UMR-5199) Laboratory at Bordeaux University, Pessac, France). A review number is not applicable, as no formal review or project number was provided at the time of approval.

The excavations of the archeological sites were conducted in the 1980s by French governmental services, such as the *Directions régionales des Antiquités Historiques (DRAH) et Préhistoriques (DRAP*), which later became the *Services régionaux de l'archéologie*, as well as the *Services d'archéologie municipaux* of certain cities. The excavated human remains were subsequently entrusted to and valorized by the former laboratory Origine et Évolution d'H*omo sapiens* (UA 376), at Bordeaux University 1, where they were studied and incorporated into the teaching collection. Following several institutional re-organizations, this laboratory became the present PACEA laboratory at Bordeaux University, where the remains are currently curated.

It was not possible to identify descendant communities associated with the human remains analyzed in this research. The remains were recovered from ossuary pits—secondary deposits resulting from burial ground re-use and re-organization—which had lost their original burial contexts. As a result, the identities of the individuals could not be determined, nor could connections to specific descendant communities be established.

All authors of this study are affiliated with French higher education and research institutions, and two of the four authors are French nationals. This ensured that the research was conducted with local expertise and collaboration.

The images presented are 3D representations of the original human remains, essential for accurately illustrating the methodological protocol used in this research.

Conflicts of Interest

The authors declare no conflicts of interest.

Data Availability Statement

The reference 3D model is accessible for download in the MorphoSource repository, free to download (https://www.morphosource.org/concern/media/000691022; https://n2t.net/ark:/87602/m4/691022). The described scripts for protocol execution, accompanied by a detailed explanation of their functionality, are provided in the Supporting Information (S3–S7, S11). The full code is also available on Github (https://github.com/ElleLiagre/medial-epicondyle-cropping-protocol), where more recent versions may be available. The R code used to perform the statistical analyses on the dataset, as well as the raw data and detailed results of the reliability assessments are provided in the Supporting Information (S8–S10, S12–S14).

References

Abdel Fatah, E. E., N. R. Shirley, M. R. Mahfouz, and B. M. Auerbach. 2012. "A Three-Dimensional Analysis of Bilateral Directional Asymmetry in the Human Clavicle." *American Journal of Physical Anthropology* 149, no. 4: 547–559. https://doi.org/10.1002/ajpa.22156.

al-Oumaoui, I., S. Jiménez-Brobeil, and P. Du Souich. 2004. "Markers of Activity Patterns in Some Populations of the Iberian Peninsula." *International Journal of Osteoarchaeology* 14, no. 5: 343–359. https://doi.org/10.1002/oa.719.

Altman, D. G. 1999. *Practical Statistics for Medical Research*. Chapman & Hall/CRC.

Benjamin, M., A. Rufai, and J. R. Ralphs. 2000. "The Mechanism of Formation of Bony Spurs (Enthesophytes) in the Achilles Tendon." *Arthritis & Rheumatism* 43, no. 3: 576. https://doi.org/10.1002/1529-0131(200003)43:3<576::AID-ANR14>3.0.CO;2-A.

Benjamin, M., H. Toumi, J. R. Ralphs, G. Bydder, T. M. Best, and S. Milz. 2006. "Where Tendons and Ligaments Meet Bone: Attachment Sites ('Entheses') in Relation to Exercise and/or Mechanical Load." *Journal of Anatomy* 208, no. 4: 471–490. https://doi.org/10.1111/j.1469-7580.2006.00540.x.

Bourreau, J. 2021. "Proposition d'une méthode qualitative d'enregistrement des changements enthésiques au niveau de l'attache proximale du ligament collatéral médial de l'humérus et hypothèse étiologique." Master thesis, Université de Bordeaux.

Bousquié, L., F. A. Karakostis, I. Crevecoeur, and S. Villotte. 2022. "Technical Note: Investigating Activity-Induced 3d Hand Entheseal Variation in a Documented South African Sample." *Archaeological and Anthropological Sciences* 14, no. 11: 213. https://doi.org/10.1007/s12520-022-01677-1.

Bucchi, A., J. Luengo, A. Del Bove, and C. Lorenzo. 2020. "Insertion Sites in Manual Proximal Phalanges of African Apes and Modern Humans." *American Journal of Physical Anthropology* 173, no. 3: 556–567. https://doi.org/10.1002/ajpa.24127.

Buck, F. M., C. S. Zoner, F. Cardoso, et al. 2010. "Can Osseous Landmarks in the Distal Medial Humerus Be Used to Identify the Attachment Sites of Ligaments and Tendons: Paleopathologic–Anatomic Imaging Study in Cadavers." *Skeletal Radiology* 39, no. 9: 905–913. https://doi.org/10.1007/s00256-009-0799-2.

Bucknor, M. D., K. J. Stevens, and L. S. Steinbach. 2016. "Elbow Imaging in Sport: Sports Imaging Series." *Radiology* 279, no. 1: 12–28. https://doi.org/10.1148/radiol.2016150501.

Capasso, L., L. Pierfelice, E. Michetti, A. D. Fabrizio, and R. D'Anastasio. 2004. "Lesions Linked to Athletic Activities in the Ancient Roman Population From Herculaneum (Italy, First Century AD)." *L'Anthropologie* 42: 181–187.

Casado, A., V. Punsola, M. Gómez, et al. 2019. "Three-Dimensional Geometric Morphometric Analysis of the Distal Radius Insertion Sites of the Palmar Radiocarpal Ligaments in Hominoid Primates." *American Journal of Physical Anthropology* 170, no. 1: 24–36. https://doi.org/10.1002/ajpa.23885.

Castro, A. A., F. A. Karakostis, L. E. Copes, et al. 2022. "Effects of Selective Breeding for Voluntary Exercise, Chronic Exercise, and Their Interaction on Muscle Attachment Site Morphology in House Mice." *Journal of Anatomy* 240, no. 2: 279–295. https://doi.org/10.1111/joa.13547.

Chen, J., and X. Zhang. 2022. "dICC: Distance-Based Intraclass Correlation Coefficient for Metagenomic Reproducibility Studies." *Bioinformatics* 38, no. 21: 4969–4971. https://doi.org/10.1093/bioinformatics/btac618.

Chen, Y., X. Zhang, L. Yang, and L. Zhang. 2023. *GUniFrac: Generalized UniFrac Distances, Distance-Based Multivariate Methods and Feature-Based Univariate Methods for Microbiome Data Analysis* (Version 1.8) [R package]. CRAN.

Churchill, S. E., and A. G. Morris. 1998. "Muscle Marking Morphology and Labour Intensity in Prehistoric Khoisan Foragers." *International Journal of Osteoarchaeology* 8, no. 5: 390–411. https://doi.org/10.1002/(SICI)1099-1212(1998090)8:5<390::AID-OA435>3.0.CO;2-N.

Churchill, S. E., and J. A. Rhodes. 2009. "The Evolution of the Human Capacity for "Killing at a Distance": The Human Fossil Evidence for the

Evolution of Projectile Weaponry." In *The Evolution of Hominin Diets*, edited by J.-J. Hublin and M. P. Richards, 201–210. Springer.

Ciccotti, M. C., M. A. Schwartz, and M. G. Ciccotti. 2004. "Diagnosis and Treatment of Medial Epicondylitis of the Elbow." *Clinics in Sports Medicine* 23, no. 4: 693–705. https://doi.org/10.1016/j.csm.2004.04.011.

Cignoni, P., M. Callieri, M. Corsini, M. Dellepiane, F. Ganovelli, and G. Ranzuglia. 2008. "MeshLab: An Open-Source Mesh Processing Tool." Europgraphics Italian Chapter Conference, 8.

Corner, B. D., S. Lele, and J. T. Richtsmeier. 1992. "Measuring Precision of Three-Dimensional Landmark Data." *Journal of Quantitative Anthropology* 3: 347–359.

Corron, L. K., K. A. Broehl, E. Y. Chu, et al. 2022. "Agreement and Error Rates Associated With Standardized Data Collection Protocols for Skeletal and Dental Data on 3D Virtual Subadult Crania." *Forensic Science International* 334: 111272. https://doi.org/10.1016/j.forsciint.2022.111272.

Daruwalla, J. H., C. A. Daly, and J. G. Seiler. 2017. "Medial Elbow Injuries in the Throwing Athlete." *Hand Clinics* 33, no. 1: 47–62. https://doi.org/10.1016/j.hcl.2016.08.013.

Davis, C. B., K. A. Shuler, M. E. Danforth, and K. E. Herndon. 2013. "Patterns of Interobserver Error in the Scoring of Entheseal Changes." *International Journal of Osteoarchaeology* 23, no. 2: 147–151. https://doi.org/10.1002/oa.2277.

Dutour, O. 1986. "Enthesopathies (Lesions of Muscular Insertions) as Indicators of the Activities of Neolithic Saharan Populations." *American Journal of Physical Anthropology* 71, no. 2: 221–224. https://doi.org/10.1002/ajpa.1330710209.

Dutour, O. 2000. "Chasse et activités physiques dans la Préhistoire: Les marqueurs osseuxd'activités chez l'homme fossile." *Anthropologie et Préhistoire* 111: 156–165.

Fedorov, A., R. Beichel, J. Kalpathy-Cramer, et al. 2012. "3D Slicer as an Image Computing Platform for the Quantitative Imaging Network." *Magnetic Resonance Imaging* 30, no. 9: 1323–1341. https://doi.org/10.1016/j.mri.2012.05.001.

Feuerriegel, E. M. 2016. "Biomechanics of the Hominin Upper Limb: Entheseal Development and Stone Tool Manufacture." PhD thesis, Australian National University.

Fuss, F. K. 1991. "The Ulnar Collateral Ligament of the Human Elbow Joint. Anatomy, Function and Biomechanics." *Journal of Anatomy* 175: 203–212.

Gamer, M., J. Lemon, I. Fellows, and P. Singh. 2012. *Irr: Various Coefficients of Interrater Reliability and Agreement* (Version 0.84.1) [R package]. CRAN.

Gunz, P., P. Mitteroecker, S. Neubauer, G. W. Weber, and F. L. Bookstein. 2009. "Principles for the Virtual Reconstruction of Hominin Crania." *Journal of Human Evolution* 57, no. 1: 48–62. https://doi.org/10.1016/j.jhevol.2009.04.004.

Hawkey, D. E., and C. F. Merbs. 1995. "Activity-Induced Musculoskeletal Stress Markers (MSM) and Subsistence Strategy Changes Among Ancient Hudson Bay Eskimos." *International Journal of Osteoarchaeology* 5, no. 4: 324–338. https://doi.org/10.1002/oa.1390050403.

Henderson, C. Y. 2013. "Technical Note: Quantifying Size and Shape of Entheses." *Anthropological Science* 121, no. 1: 63–73. https://doi.org/10.1537/ase.121017.

Hirst, C. S., S. White, and S. E. Smith. 2018. "Standardisation in 3D Geometric Morphometrics: Ethics, Ownership, and Methods." *Archaeologies* 14, no. 2: 272–298. https://doi.org/10.1007/s11759-018-9349-7.

Horbaly, H. 2023. "Covariance in Human Limb Joint Articular Morphology." *American Journal of Biological Anthropology* 182, no. 3: 401–411. https://doi.org/10.1002/ajpa.24826.

Ibáñez-Gimeno, P., I. Galtés, X. Jordana, E. Fiorin, J. Manyosa, and A. Malgosa. 2013. "Entheseal Changes and Functional Implications of the Humeral Medial Epicondyle: Functional Implications of the Humeral Medial Epicondyle." *International Journal of Osteoarchaeology* 23, no. 2: 211–220. https://doi.org/10.1002/oa.2299.

Ieng, J., F. A. Karakostis, and C. Wilczak. 2024. "Applying the V.E.R.A. Method to Entheses of the Humerus: An Assessment of Repeatability and Reproducibility." *International Journal of Osteoarchaeology* 34: e3341. https://doi.org/10.1002/oa.3341.

Ikezu, M., M. Edama, K. Matsuzawa, et al. 2020. "Morphological Features of the Ulnar Collateral Ligament of the Elbow and Common Tendon of Flexor-Pronator Muscles." *Orthopaedic Journal of Sports Medicine* 8, no. 9: 232596712095241. https://doi.org/10.1177/2325967120952415.

Jani, G., A. Johnson, U. Parekh, T. Thompson, and A. Pandey. 2020. "Effective Approaches to Three-Dimensional Digital Reconstruction of Fragmented Human Skeletal Remains Using Laser Surface Scanning." *Forensic Science International: Synergy* 2: 215–223. https://doi.org/10.1016/j.fsisyn.2020.07.002.

Karakostis, F. A. 2025. "Introducing "Validated Entheses-Based Reconstruction of Activity 2.0" (VERA 2.0): Semi-Automated 3D Analysis of Bone Surface Changes." *PLoS One* 20, no. 4: e0321479. https://doi.org/10.1371/journal.pone.0321479.

Karakostis, F. A., and K. Harvati. 2021. "New Horizons in Reconstructing Past Human Behavior: Introducing the "Tübingen University Validated Entheses-Based Reconstruction of Activity" Method." *Evolutionary Anthropology: Issues, News, and Reviews* 30, no. 3: 185–198. https://doi.org/10.1002/evan.21892.

Karakostis, F. A., and G. Hotz. 2024. "Reflections of Manual Labor in the Hand Entheses of Early Industrial Women Workers With Extensively Documented Life Histories." *American Journal of Biological Anthropology* 183, no. 3: e24636. https://doi.org/10.1002/ajpa.24636.

Karakostis, F. A., G. Hotz, H. Scherf, J. Wahl, and K. Harvati. 2018. "A Repeatable Geometric Morphometric Approach to the Analysis of Hand Entheseal Three-Dimensional Form." *American Journal of Physical Anthropology* 166, no. 1: 246–260. https://doi.org/10.1002/ajpa.23421.

Karakostis, F. A., and C. Lorenzo. 2016. "Morphometric Patterns Among the 3D Surface Areas of Human Hand Entheses." *American Journal of Physical Anthropology* 160, no. 4: 694–707. https://doi.org/10.1002/ajpa.22999.

Kennedy, K. A. 1983. "Morphological Variations in Ulnar Supinator Crests and Fossae as Identifying Markers of Occupational Stress." *Journal of Forensic Sciences* 28, no. 4: 871–876.

Knüsel, C. J. 2011. "Men Take up Arms for War. Sex and Status Distinctions of Humeral Medial Epicondylar Avulsion Fractures in the Archaeological Record." In *Breathing New Life Into the Evidence of Death: Contemporary Approaches to Bioarchaeology*, edited by A. Baadsgaard, A. T. Boutin, and J. E. Buikstra, 221–250. School for Advanced Research Press.

Koo, T. K., and M. Y. Li. 2016. "A Guideline of Selecting and Reporting Intraclass Correlation Coefficients for Reliability Research." *Journal of Chiropractic Medicine* 15, no. 2: 155–163. https://doi.org/10.1016/j.jcm.2016.02.012.

Kunze, J., K. Harvati, G. Hotz, and F. A. Karakostis. 2024. "Humanlike Manual Activities in Australopithecus." *Journal of Human Evolution* 196: 103591. https://doi.org/10.1016/j.jhevol.2024.103591.

Kunze, J., F. A. Karakostis, S. Merker, et al. 2022. "Entheseal Patterns Suggest Habitual Tool Use in Early Hominins." *PaleoAnthropology* 2022, no. 2: 195–210. https://doi.org/10.48738/2022.ISS2.61.

Labott, J. R., W. R. Aibinder, J. S. Dines, and C. L. Camp. 2018. "Understanding the Medial Ulnar Collateral Ligament of the Elbow:

Review of Native Ligament Anatomy and Function." *World Journal of Orthopedics* 9, no. 6: 78–84. https://doi.org/10.5312/wjo.v9.i6.78.

Lautenschlager, S. 2016. "Reconstructing the Past: Methods and Techniques for the Digital Restoration of Fossils." *Royal Society Open Science* 3, no. 10: 160342. https://doi.org/10.1098/rsos.160342.

Lin, L. I.-K. 1989. "A Concordance Correlation Coefficient to Evaluate Reproducibility." *Biometrics* 45, no. 1: 255. https://doi.org/10.2307/2532051.

Mariotti, V., F. Facchini, and M. G. Belcastro. 2004. "Enthesopathies—Proposal of a Standardized Scoring Method and Applications." *Collegium Antropologicum* 15: 145–159.

Mariotti, V., F. Facchini, and M. G. Belcastro. 2007. "The Study of Entheses: Proposal of a Standardised Scoring Method for Twenty-Three Entheses of the Postcranial Skeleton." *Collegium Antropologicum* 31, no. 1: 291–313.

McBride, G. B. 2005. "A Proposal for Strength-of-Agreement Criteria for Lin's Concordance Correlation Coefficient." In *NIWA Client Report: HAM2005-062*, vol. 45, 307–310. National Institue of Water & Atmospheric Research Ltd.

Milz, S., T. Tisher, A. Buettner, et al. 2004. "Molecular Composition and Pathology of Entheses on the Medial and Lateral Epicondyles of the Humerus: A Structural Basis for Epicondylitis." *Annals of the Rheumatic Diseases* 63, no. 9: 1015–1021. https://doi.org/10.1136/ard.2003.016378.

Nakanishi, K., T. Masatomi, T. Ochi, et al. 1996. "MR Arthrography of Elbow: Evaluation of the Ulnar Collateral Ligament of Elbow." *Skeletal Radiology* 25, no. 7: 629–634. https://doi.org/10.1007/s002560050149.

Netter, F. H. 2019. *The Atlas of Human Anatomy*. 7th ed. Elsevier.

Nikita, E., P. Xanthopoulou, A. Bertsatos, M. Chovalopoulou, and I. Hafez. 2019. "A Three-Dimensional Digital Microscopic Investigation of Entheseal Changes as Skeletal Activity Markers." *American Journal of Physical Anthropology* 169: 704–713. https://doi.org/10.1002/ajpa.23850.

Noldner, L. K., and H. J. H. Edgar. 2013. "3D Representation and Analysis of Enthesis Morphology." *American Journal of Physical Anthropology* 152, no. 3: 417–424. https://doi.org/10.1002/ajpa.22367.

Nolte, M., and C. Wilczak. 2013. "Three-Dimensional Surface Area of the Distal Biceps Enthesis, Relationship to Body Size, Sex, Age and Secular Changes in a 20th Century American Sample: Surface Area of the Biceps Enthesis." *International Journal of Osteoarchaeology* 23, no. 2: 163–174. https://doi.org/10.1002/oa.2292.

Olszewski, R., H. Reychler, G. Cosnard, J. M. Denis, S. Vynckier, and F. Zech. 2008. "Accuracy of Three-Dimensional (3D) Craniofacial Cephalometric Landmarks on a Low-Dose 3D Computed Tomograph." *Dento Maxillo Facial Radiology* 37, no. 5: 261–267. https://doi.org/10.1259/dmfr/33343444.

Pany, D., B. Viola, and M. Teschler-Nicola. 2008. "Analysis of Musculoskeletal Stress Markers and Joint Disease on the Early Medieval Skeletons From Thunau." *American Journal of Physical Anthropology* 135: 167–168.

Patel, R. M., T. S. Lynch, N. H. Amin, G. Calabrese, S. M. Gryzlo, and M. S. Schickendantz. 2014. "The Thrower's Elbow." *Orthopedic Clinics of North America* 45, no. 3: 355–376. https://doi.org/10.1016/j.ocl.2014.03.007.

Perchalski, B., A. Placke, S. M. Sukhdeo, et al. 2018. "Asymmetry in the Cortical and Trabecular Bone of the Human Humerus During Development." *Anatomical Record* 301, no. 6: 1012–1025. https://doi.org/10.1002/ar.23705.

Polet, C., M. L. Martiarena, S. Villotte, and M. Vercauteren. 2019. "Throwing Activities Among Neolithic Populations From the Meuse River Basin (Belgium, 4500–2500 BC) With a Focus on Adolescents." *Childhood in the Past* 12, no. 2: 81–95. https://doi.org/10.1080/17585716.2019.1638555.

Porto, A., S. Rolfe, and A. M. Maga. 2021. "ALPACA: A Fast and Accurate Computer Vision Approach for Automated Landmarking of Three-Dimensional Biological Structures." *Methods in Ecology and Evolution* 12, no. 11: 2129–2144. https://doi.org/10.1111/2041-210X.13689.

Posit team. 2024. *RStudio: Integrated Development Environment for R*. Posit Software, PBC.

Profico, A., C. Zeppilli, I. Micarelli, et al. 2021. "Morphometric Maps of Bilateral Asymmetry in the Human Humerus: An Implementation in the R Package Morphomap." *Symmetry* 13, no. 9: 1711. https://doi.org/10.3390/sym13091711.

R Core Team. 2023. *R: A Language and Environment for Statistical Computing*. R Foundation for Statistical Computing.

Rhodes, J. A., and S. E. Churchill. 2009. "Throwing in the Middle and Upper Paleolithic: Inferences From an Analysis of Humeral Retroversion." *Journal of Human Evolution* 56, no. 1: 1–10. https://doi.org/10.1016/j.jhevol.2008.08.022.

Rhodes, J. A., and C. J. Knüsel. 2005. "Activity-Related Skeletal Change in Medieval Humeri: Cross-Sectional and Architectural Alterations." *American Journal of Physical Anthropology* 128, no. 3: 536–546. https://doi.org/10.1002/ajpa.20147.

Robb, J. E. 1998. "The Interpretation of Skeletal Muscle Sites: A Statistical Approach." *International Journal of Osteoarchaeology* 8, no. 5: 363–377. https://doi.org/10.1002/(SICI)1099-1212(1998090)8:5<363::AID-OA438>3.0.CO;2-K.

Ross, A. H., and S. Williams. 2008. "Testing Repeatability and Error of Coordinate Landmark Data Acquired From Crania*." *Journal of Forensic Sciences* 53, no. 4: 782–785. https://doi.org/10.1111/j.1556-4029.2008.00751.x.

Scherf, H., J. Wahl, J. Hublin, and K. Harvati. 2016. "Patterns of Activity Adaptation in Humeral Trabecular Bone in Neolithic Humans and Present-Day People." *American Journal of Physical Anthropology* 159, no. 1: 106–115. https://doi.org/10.1002/ajpa.22835.

Schlager, S. 2017. "Chapter 9—Morpho and Rvcg—Shape Analysis in R: R-Packages for Geometric Morphometrics, Shape Analysis and Surface Manipulations." In *Statistical Shape and Deformation Analysis*, edited by G. Zheng, S. Li, and G. Székely, 217–256. Academic Press.

Shaw, C. N., C. L. Hofmann, M. D. Petraglia, J. T. Stock, and J. S. Gottschall. 2012. "Neandertal Humeri May Reflect Adaptation to Scraping Tasks, but Not Spear Thrusting." *PLoS One* 7, no. 7: e40349. https://doi.org/10.1371/journal.pone.0040349.

Shaw, C. N., and J. T. Stock. 2009. "Habitual Throwing and Swimming Correspond With Upper Limb Diaphyseal Strength and Shape in Modern Human Athletes." *American Journal of Physical Anthropology* 140, no. 1: 160–172. https://doi.org/10.1002/ajpa.21063.

Shearer, B. M., S. B. Cooke, L. B. Halenar, et al. 2017. "Evaluating Causes of Error in Landmark-Based Data Collection Using Scanners." *PLoS One* 12, no. 11: e0187452. https://doi.org/10.1371/journal.pone.0187452.

Shiri, R., and E. Viikari-Juntura. 2011. "Lateral and Medial Epicondylitis: Role of Occupational Factors." *Best Practice & Research Clinical Rheumatology* 25, no. 1: 43–57. https://doi.org/10.1016/j.berh.2011.01.013.

Signorell, A. 2024. *DescTools: Tools for Descriptive Statistics* (Version 0.99.57) [R package]. CRAN.

Sládek, V., M. Hora, K. Farkašová, and T. R. Rocek. 2016. "Impact of Grinding Technology on Bilateral Asymmetry in Muscle Activity of the Upper Limb." *Journal of Archaeological Science* 72: 142–156. https://doi.org/10.1016/j.jas.2016.07.001.

Sládek, V., C. B. Ruff, M. Berner, et al. 2016. "The Impact of Subsistence Changes on Humeral Bilateral Asymmetry in Terminal Pleistocene and Holocene Europe." *Journal of Human Evolution* 92: 37–49. https://doi.org/10.1016/j.jhevol.2015.12.001.

Sparacello, V. S., S. Villotte, L. L. Shackelford, and E. Trinkaus. 2017. "Patterns of Humeral Asymmetry Among Late Pleistocene Humans." *Comptes Rendus Palevol* 16, no. 5–6: 680–689. https://doi.org/10.1016/j.crpv.2016.09.001.

Stirland, A. J. 1993. "Asymmetry and Activity-Related Change in the Male Humerus." *International Journal of Osteoarchaeology* 3, no. 2: 105–113. https://doi.org/10.1002/oa.1390030207.

Tallman, M. 2013. "Forelimb to Hindlimb Shape Covariance in Extant Hominoids and Fossil Hominins." *Anatomical Record* 296, no. 2: 290–304. https://doi.org/10.1002/ar.22624.

Trinkaus, E., S. E. Churchill, and C. B. Ruff. 1994. "Postcranial Robusticity in Homo. II: Humeral Bilateral Asymmetry and Bone Plasticity." *American Journal of Physical Anthropology* 93, no. 1: 1–34. https://doi.org/10.1002/ajpa.1330930102.

Turcotte, C. M., K. N. Rabey, D. J. Green, and S. C. McFarlin. 2022. "Muscle Attachment Sites and Behavioral Reconstruction: An Experimental Test of Muscle-Bone Structural Response to Habitual Activity." *American Journal of Biological Anthropology* 177, no. 1: 63–82. https://doi.org/10.1002/ajpa.24410.

Vance, V. L., and M. Steyn. 2013. "Geometric Morphometric Assessment of Sexually Dimorphic Characteristics of the Distal Humerus." *Homo* 64, no. 5: 329–340. https://doi.org/10.1016/j.jchb.2013.04.003.

Vangsness, C. T., and F. W. Jobe. 1991. "Surgical Treatment of Medial Epicondylitis. Results in 35 Elbows." *Journal of Bone and Joint Surgery. British Volume* 73, no. 3: 409–411. https://doi.org/10.1302/0301-620X.73B3.1670439.

Varalli, A., S. Villotte, I. Dori, and V. S. Sparacello. 2020. "New Insights Into Activity-Related Functional Bone Adaptations and Alterations in Neolithic Liguria (Northwestern Italy)." *Bulletins et Mémoires de la Société d'Anthropologie de Paris* 32, no. 1–2: 34–58. https://doi.org/10.3166/bmsap-2020-0072.

Villotte, S. 2006. "Connaissances médicales actuelles, cotation des enthésopathies: Nouvelle méthode." *Bulletins et Mémoires de la Société d'Anthropologie de Paris* 18, no. 1–2: 65–85. https://doi.org/10.4000/bmsap.1325.

Villotte, S., S. E. Churchill, O. J. Dutour, and D. Henry-Gambier. 2010. "Subsistence Activities and the Sexual Division of Labor in the European Upper Paleolithic and Mesolithic: Evidence From Upper Limb Enthesopathies." *Journal of Human Evolution* 59, no. 1: 35–43. https://doi.org/10.1016/j.jhevol.2010.02.001.

Villotte, S., and C. J. Knüsel. 2014. ""I Sing of Arms and of a Man...": Medial Epicondylosis and the Sexual Division of Labour in Prehistoric Europe." *Journal of Archaeological Science* 43: 168–174. https://doi.org/10.1016/j.jas.2013.12.009.

Von Cramon-Taubadel, N., B. C. Frazier, and M. M. Lahr. 2007. "The Problem of Assessing Landmark Error in Geometric Morphometrics: Theory, Methods, and Modifications." *American Journal of Physical Anthropology* 134, no. 1: 24–35. https://doi.org/10.1002/ajpa.20616.

Walker-Bone, K., K. T. Palmer, I. Reading, D. Coggon, and C. Cooper. 2012. "Occupation and Epicondylitis: A Population-Based Study." *Rheumatology* 51, no. 2: 305–310. https://doi.org/10.1093/rheumatology/ker228.

Wallace, I. J., J. M. Winchester, A. Su, D. M. Boyer, and N. Konow. 2017. "Physical Activity Alters Limb Bone Structure but Not Entheseal Morphology." *Journal of Human Evolution* 107: 14–18. https://doi.org/10.1016/j.jhevol.2017.02.001.

Weiss, E. 2015. "The Surface of Bones: Methods of Recording Entheseal Changes." *Surface Topography: Metrology and Properties* 3, no. 3: 034003. https://doi.org/10.1088/2051-672X/3/3/034003.

Wilczak, C. A. 1998. "Consideration of Sexual Dimorphism, Age, and Asymmetry in Quantitative Measurements of Muscle Insertion Sites." *International Journal of Osteoarchaeology* 8, no. 5: 311–325. https://doi.org/10.1002/(SICI)1099-1212(1998090)8:5<311::AID-OA443>3.0.CO;2-E.

Williams-Hatala, E. M., K. G. Hatala, S. Hiles, and K. N. Rabey. 2016. "Morphology of Muscle Attachment Sites in the Modern Human Hand Does Not Reflect Muscle Architecture." *Scientific Reports* 6, no. 1: 28353. https://doi.org/10.1038/srep28353.

Zumwalt, A. 2005. "A New Method for Quantifying the Complexity of Muscle Attachment Sites." *Anatomical Record Part B: The New Anatomist* 286B, no. 1: 21–28. https://doi.org/10.1002/ar.b.20075.

Supporting Information

Additional supporting information can be found online in the Supporting Information section. **Data S1.** Detailed Information about the Study Sample. **Data S2.** Technical Details of 3D Model Pre-Processing and the Cropping Protocol. **Data S3.** Python Script "batchRemeshing.py". **Data S4**. Python Script "batchMirroring.py". **Data S5**. Python Script "batchAlign.py". **Data S6**. Python Script "crop.py". **Data S7**. Python Script "batchCrop.py". **Data S8.** Visual Outcomes of the Cropping Protocol Applied to the Study Sample. **Data S9.** Detailed Results of the Statistical Tests on Landmark Placement. **Data S10.** Detailed Results of the Statistical Tests on 3D Surface Area of Cropped Models. **Data S11.** User Guide for the Humeral Medial Cropping Protocol: A Step-by-Step Manual. **Data S12.** Raw data of the Landmark Coordinates. **Data S13.** Raw data of the 3D Surface Area of Cropped Models. **Data S14.** R Script for Statistical Analyses.